Constructing MRI-based 3D precise human hand models for product ergonomic assessments

Yasutomo Shimizu*, Keisuke Kawaguchi and Satoshi Kanai
Division of Systems Science and Informatics,
Graduate School of Information Science and Technology, Hokkaido University,
Sapporo, Japan

Abstract

Since human hands play an important role in grasping and manipulating the product, the digital hand model which can reproduce the structure and the motion of the human hand with high-precision is very useful for virtual ergonomic assessment of the product. The purpose of this study is to develop a new method of MRI-based modeling of a digital hand whose precision is sufficient to reproduce virtual grasp postures for ergonomic assessments. The digital hand has 3D models of the bones and a skin surface extracted from MRI data. The bone link model has 2-DOF finger joint motion which can precisely approximate real motions using ICP algorithm and quaternion interpolation. And a skin surface deformation method can accurately reproduce the skin surface deformation around the ball of the thumb using the combination of traditional SSD (skeletal-subspace deformation) and RBF interpolation. The comparison of the simulated contact area of our hand model with the real one showed the effectiveness of the proposed model.

Key words: Ergonomic Assessment, MRI, Digital Hand, Joint Motion, Skin Deformation

1. Introduction

Recently, ergonomic assessments even for hand-held products or parts such as mobile phones, cameras, beverage containers are becoming important to gain their market competitiveness. Conventional ergonomic assessments are carried out in the form of user-tests which need many human subjects and the physical mockups. Unfortunately, fabricating physical mockups and ensuring sufficient number of subjects costs much, and subjective evaluations are only obtained from the tests which are insufficient for quantitative and objective evaluation of ergonomics and for their redesign.

Virtual ergonomic assessment for hand-held products have been recently studied to reduce the prototyping and user-test costs, and to perform quantitative and objective assessments of quality of grasping the products. In these studies, both a precise 3D model of a human hand and a 3D CAD model of the product were first built in a computer, and virtual grasp posture is then generated automatically or manually. A few of them already implemented functions of assessing quality of grasp at virtual grasp postures. Force closure and 3D grasp quality which were originally introduced as the metrics of robotic grasping were already used for evaluating grasp postures of human hands[1,2] and for selecting desirable virtual grasp postures[3]. The other metrics of assessing quality of grasp have been also studied based-on dynamics[4], finger-joint angle distribution [5,6] and grasp fitness between finger shape and product shape[7].

A precise 3D model of a human hand called *digital hand*, which can accurately reproduce the finger motion and skin deformation of human hand at virtual grasp postures is strongly needed in the virtual ergonomic assessment. Some researches on the human hand modeling have been done. The Japanese generic hand model was developed by Kouch[8], but the finger motion was not verified. Kurihara[9] proposed a precise 3D bone

* Corresponding author email: y_shimizu@sdm.ssi.ist.hokudai.ac.jp

link model and surface skin model from X-ray CT scan, but their finger joint angle had many redundant D.O.Fs. which is not necessarily suitable of generating virtual grasp postures. Miyata[10] also developed the finger joint models from MRI images, but only the 1 D.O.F motion of flexion/extension at DIP, PIP and IP joints were modeled, and 2 D.O.F joint motion of thumb which is most important for realizing the oppositions of the human grasp was ignored. Therefore, the digital hands in previous researches could not fully approximant the 3D motion of thumb carpometacarpal (CMC) joint and the skin surface deformation around the ball of the thumb caused by the joint's motion.

In this paper, we propose a new method of MRI-based modeling of a digital hand whose precision is sufficient to reproduce virtual grasp postures for ergonomic assessments.

2. Human hand modeling methods

2.1. Outline of the human hand modeling method

The digital hand model in our study mainly consist of a *bone link model* and a *skin surface model*[7]. Both models are created from MRI measurements of a real human hand by using the proposed method. The outline of the method is shown in Fig. 1.

I. Multiple postures of a subject's hand shown in Figure 3 is measured by MRI (Fig. 1-A1).

II. 3D triangle mesh of bones and a skin of a hand are extracted from the MRI images using a Marching cubes, and there noise in the images is eliminated and the vertex positions of the models are smoothed(Fig. 1-A2).

III. Relative positions and orientations of meshes of a particular bone at different postures are matched each other using ICP algorithm. A single rotation or quaternion interpolation joint motion is derived from the obtained 3D transformation, the calculated center of rotations and the rotation axis direction [9][10] in order to complete the bone link model (Fig. 1-A3).

IV. A portion of the vertices of the skin surface model is assigned to a certain bone automatically to enable the surface skin deformation using skeletal-subspace deformation (SSD). Moreover, by comparing the deformed skin surface simulated by SSD to an actual skin at the flexion, the accuracy of skin

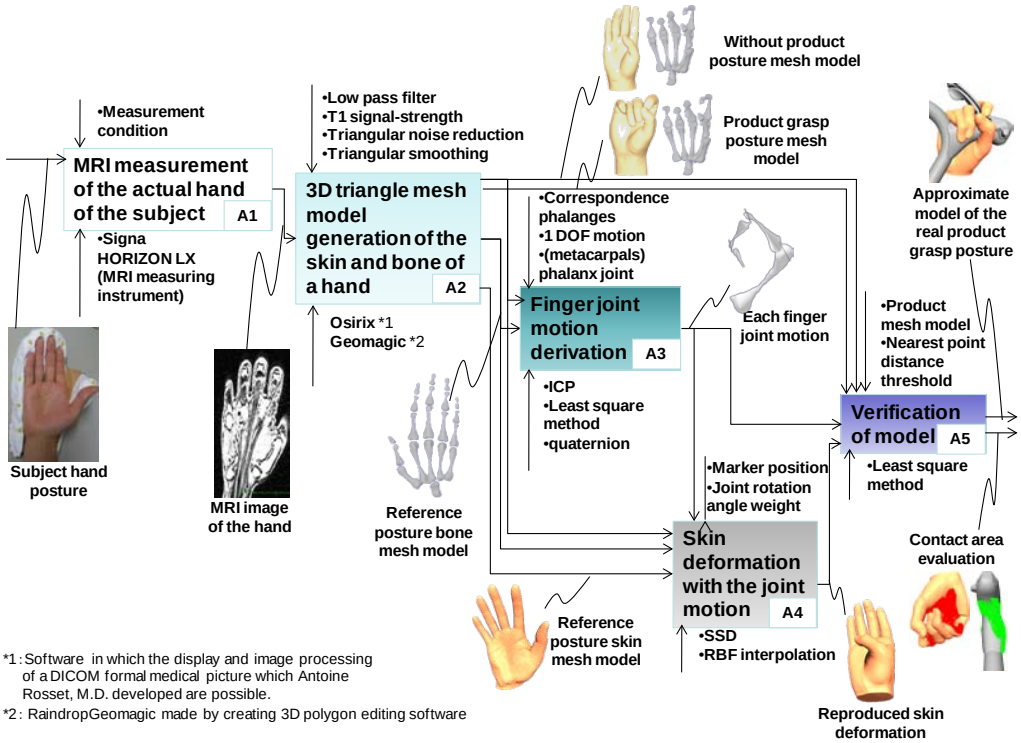

Fig. 1. Outline of proposal method.

deformation around the ball of the thumb is improved by applying RBF interpolation to SSD [9](Fig. 1-A4).

V. For the bone link model and the surface skin model derived in III and IV, precision verification is performed. The motion errors of the bones and grasp contact area are evaluated (Fig. 1-A5).

2.2. Structure of bone link model

The bone link model in this study has the link and joint structures shown in Fig. 2. The degrees of freedom (DOF) of the joint structures are modeled based on anatomical knowledge [11]. Each metacarpophalangeal (MP) joint of four fingers has 2DOF rotations; flexion/extension and adduction/abduction. Each proximal interphalangeal (PIP) joint and distal interphalangeal(DIP) joint of them has 1DOF rotation of flexion/extension. While the CMC joint of a thumb has 2DOF where both flexion/extension and adduction/abduction accompanied with pronation/supination motions cannot be simply modeled as simple rotations. The MP and IP joints of a thumb have 1DOF of simple rotation.

2.3. MRI measurement of a subject's hand

MRI measurement is performed with multiple postures as shown in Fig. 3 for two male subjects without any medical injuries in their hands. The measurement condition is shown in Table 1. 12 small markers of 5mm diameter are placed on the skin around the ball of the thumb when the postures of Fig. 3 (a) and (b-1) ~ (b-4) are measured to acquire the actual skin surface deformations.

2.4. 3D triangle mesh model generation of the bone and skin of hand

In order to extract the 3D triangle mesh model obtained MRI images, medical image-processing software (Osirix [12]) and 3D mesh processing software (Geomagic [13]) are used. The MRI volume images are first smoothed by a low pass filter, and iso-surfaces of the bones and the skin surfaces are extracted respectively in the form of triangular mesh models by setting different threshold values of intensity using Marching cube. Moreover, unwanted minute objects caused by the measurement noise are deleted manually, and the mesh

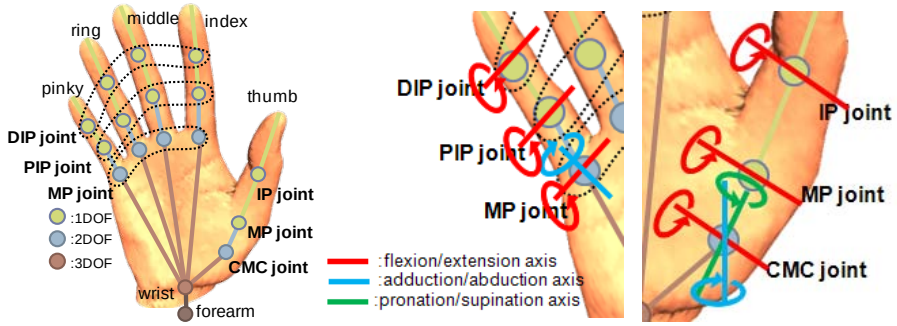

Fig. 2. Joint degree of freedom and joint axis arrangement model based on anatomical insight.

Fig. 3. MRI measurement postures.

Table 1. MRI measurement condition

Scanning image	T1 weighted magnetic resonance image
Magnetic field strength	1.5T
Resolution	256 × 256
Thickness of the slice	1.0mm
Number of slice	124
Pixel size	0.78mm
Measuring time	3min56sec
Marker	Oral refreshing capsule
Fixture device material	Paper clay

models of bones and skins are converted into subdivision surfaces to improve their surface smoothness.

2.5. Deriving finger joint motions of the bone link model

Joint motions are derived from comparing 3D positions and orientations of phalanges at different grasp postures. First, the mesh model of a phalange at the reference posture (relaxed natural posture) and the one of the same phalange at a bended posture are chosen manually in our developed software. Then the position and orientation of these two mesh models are matched together using ICP algorithm as shown in Fig. 4. The rigid body transformation matrix $\mathbf{T}^{ICP}$ which gives the minimum matching error between a vertex $v_{c(i)}^{T}$ of the model at the bended posture and its corresponding vertex v_i^S at the reference posture is derived by calculating the least square solution of the equation (1).

$$E^{ICP} = \min_{\mathbf{T}^{ICP}} \sum_{i=1}^{N_s} \left\| \mathbf{T}^{ICP} \mathbf{v}_i^s - \mathbf{v}_{c(i)}^T \right\|^2 \tag{1}$$

where N_S is the number of vertices of the model of reference posture, and $\mathbf{v}_i^S, \mathbf{v}_{c(i)}^T$ homogeneous coordinates of a vertex and its correspondence vertex.

If we assume that $\mathbf{T}^{ICP}$ can only be expressed as a single axis rotation and $\mathbf{P}_a$ is an arbitrary point on the rotational axis (a rotation center), the single axis rotation matrix $\mathbf{T}^{Axis}$ can be expressed as equation (2) where $\mathbf{R}^{ICP}$ is 3x3 rotational submatrix in $\mathbf{T}^{ICP}$.

$$\mathbf{T}^{Axis} = \begin{bmatrix} \mathbf{E} & \mathbf{P}_a \\ \mathbf{0}^T & 1 \end{bmatrix} \begin{bmatrix} \mathbf{R}^{ICP} & \mathbf{0} \\ \mathbf{0}^T & 1 \end{bmatrix} \begin{bmatrix} \mathbf{E} & -\mathbf{P}_a \\ \mathbf{0}^T & 1 \end{bmatrix} = \begin{bmatrix} \mathbf{R}^{ICP} & -\mathbf{R}^{ICP}\mathbf{P}_a + \mathbf{P}_a \\ \mathbf{0} & 1 \end{bmatrix} \tag{2}$$

Therefore, by replacing $\mathbf{T}^{ICP}$ by $\mathbf{T}^{Axis}$ in equation(1) and by finding the least square solution of $\mathbf{T}^{Axis}$ for equation (1), we can obtain the optimum rotation center $\mathbf{P}_a$ as $\mathbf{P}_a = (\mathbf{E} - \mathbf{R}^{ICP})^{-1} \mathbf{t}^{Axis}$, where $\mathbf{t}^{Axis}$ is the translation components of $\mathbf{T}^{Axis}$. Similarly, the optimum rotation axis direction can be derived from 3×3 rotational submatrix in $\mathbf{T}^{Axis}$ by solving a simple simultaneous linear equation. The derived single joint rotation axis from the models of Fig.4 is shown in Fig. 5.

On the other hand, since, as the anatomical knowledge, contact surfaces at CMC joint of a thumb is known to have saddle-like geometries as indicated in Fig.6, if we approximate the CMC joint motion as a single axis rotation, the bone link model cannot accurately reproduce the actual joint motion. Therefore, in our model, the combination of the linear interpolation of translation and the spherical linear interpolation of the quaternion is adopted as the CMC joint motion of the thumb. In the interpolations, the translation vector $\mathbf{t}^{ICP}$

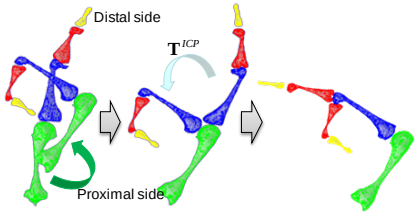

Fig. 4. ICP matching of the same phalange.

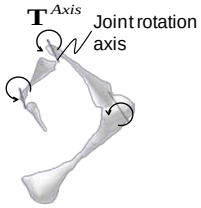

Fig. 5. The single joint rotation axis.

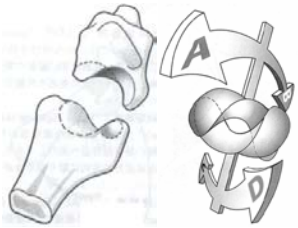

Fig. 6. The anatomical model of the thumb CMC joint.

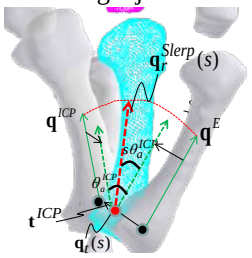

Fig. 7. Joint motion including the spherical linear interpolation by the quaternion.

of $\mathbf{T}^{ICP}$ and the quaternion expression $\mathbf{q}^{ICP}$ of the rotation component $\mathbf{R}^{ICP}$ can be simultaneously interpolated by the equations (3) and (4) using an interpolation coefficient $s(0 \le s \le 1)$ as shown in Fig. 7.

$$\mathbf{q}_t(s) = s\mathbf{t}^{ICP} \tag{3}$$

$$\mathbf{q}_r^{Slerp}(s) = \frac{\sin(1-s)\theta_a^{ICP}}{\sin\theta_a^{ICP}}\mathbf{q}^E + \frac{\sin s\theta_a^{ICP}}{\sin\theta_a^{ICP}}\mathbf{q}^{ICP} \tag{4}$$

where θ_a^{ICP} is a rotation angle about the axis of single axis of rotation derived from $\mathbf{R}^{ICP}$, $\mathbf{q}^E$ a quaternion of unit matrix, $\mathbf{q}_t(s)$ an interpolated translation vector, and $\mathbf{q}_r^{Slerp}(s)$ an interpolated quaternion.

2.6. Modeling skin deformation with the joint motions

Next, in order to reproduce accurate skin deformation especially in flexion postures, a skin deformation model along with the finger's and thumb joint motions is generated. The surfaces of four fingers and a thumb in the skin surface model are deformed followed by each joint rotation angles. The deformation is based on SSD [9] where an object surface can be smoothly deformed by rotating skeletons placed inside the object.

In our skin surface model, the vertex positions on the finger skin before and after the deformation are governed by the rotation angles of each joint, and are expressed as;

$$^{Skin}\mathbf{v}_i^{j\,\prime} = Rot(\,\mathbf{u}_{ICP},\, w_{1,i}^j w_{2,i}^j \theta^j\,)\,{}^{Skin}\mathbf{v}_i^j \tag{5}$$

where $^{Skin}\mathbf{v}_i^{j\,\prime}$, $^{Skin}\mathbf{v}_i^j$ are vertex positions after/before the deformation, $\mathbf{u}_{ICP}$ the rotation axis vector of $\mathbf{R}^{ICP}$, θ^j the rotation angle of the joint j.

$w_{1,i}^j$ and $w_{2,i}^j$ are the weights assigned to each vertex i of the skin surface model, and they express how the position of vertex i should be rotated along with the rotation of a joint j. $w_{1,i}^j$ is the weight that controls the palm side contraction and the back side extension of the surface area near the joint as shown in Fig. 8(a). The weights of vertices in the steady area are set to 0, and those in the rigid transformed area set to 1. Those in the contracted and the extended areas are assigned to the weights ranging from 0 to 1 which change linearly to the joint rotation angle. Meanwhile, $w_{2,i}^j$ is weight which sets up the amount of the influence of the j-th joint rotation on the i-th vertex, the value is predetermined based on the relative position of the vertex in two ellipses shown in Fig. 8(b), and controls of the influence of the joint rotation on the skin deformation.

Since skin surface deformation according to the motion of the thumb's CMC joint is much larger than the one according to the motion of the other joints, sufficient amount of skin deformation cannot be produced around the thumb's CMC joint only by using SSD. Therefore, the deformation shortfall generated by SSD is compensated by measuring the positions of markers placed on a real deformed skin surface at four limit postures such as flexion. In the compensation, first, the vertex on the real skin surface mesh which is closest to a marker around the ball of the thumb is selected as a *marker vertex*. The displacement between the marker vertex and the surface skin deformed only by SSD is then compensated. For this, a compensation vector is added to every vertex on the skin surface model where the displacements measured at the discrete marker

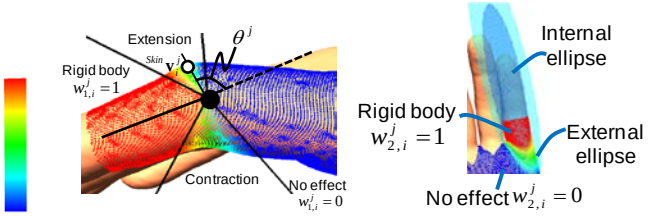

Fig. 8. Weight distribution and deformation. (a)Weighted by $w_{1,i}^j$, (b)Weighted by $w_{2,i}^j$.

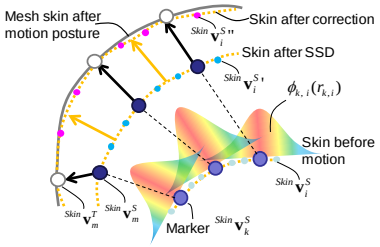

Fig. 9. RBF interpolation for skin correction.

vertices are interpolated by RBF in equation (6) (Fig. 9).

$$ {}^{Skin}\mathbf{v}_i^{S}{}'' = {}^{Skin}\mathbf{v}_i^{S}{}' + s\left(\sum_{k=1}^{N_{marker}} \phi_{k,i}(r_{k,i})\mathbf{d}_k \right) \tag{6} $$

where ${}^{Skin}\mathbf{v}_i^{S}{}''$ is a vertex position for ${}^{Skin}\mathbf{v}_i^{S}{}'$ after compensation, $r_{k,i}$ a distance from a marker vertex ${}^{Skin}\mathbf{v}_k^{S}$ to a vertex ${}^{Skin}\mathbf{v}_i^{S}$ on the skin surface model, N_{marker} the number of markers. $\phi_{k,i}(r_{k,i})$ is an exponential-type radial basis function with a constant $\beta = 3.6 \times 10^{-3}$ which is defined by equation(7).

$$ \phi_{k,i} = \exp(-\beta r_{k,i}^2) \tag{7} $$

The compensation vector $\mathbf{d}_k$ must be determined so that the marker vertex position ${}^{Skin}\mathbf{v}_m^{S}{}'$ should be identical with the one of the marker vertex ${}^{Skin}\mathbf{v}_m^{T}$ measured from MRI at a limit posture.

$$ s\left(\sum_k^{N_{mark}} \phi_{k,m}(r_{k,m})\mathbf{d}_k \right) = {}^{Skin}\mathbf{v}_m^{T} - {}^{Skin}\mathbf{v}_m^{S}{}' \tag{8} $$

This deformation compensation by RBF is only applied to the skin area near the ball of the thumb, and enables a precise skin deformation of the palm side of our digital hand.

3. Verification of the models

The average motion error of each phalange moved from the reference posture to each limit posture is shown in Table 2 and 3. For the reference, the motion errors only generated by using ICP are also indicated in the Tables which show inevitable lower limits of the errors. The errors were estimated by taking the average results of two adult male subjects (ranging aged from 22 to 24 years).

From Table 2, the average motion errors of the four fingers generated by our proposed method (single axis rotation) became 0.44~1.06 mm, and the difference in the errors between the ICP and our method did 0.15mm or less. On the other hand, from Table 3, the average motion errors of the thumb generated by the single axis

Table 2. Four fingers: average motion error at the time of each limit posture motion [mm].

	Flexion posture			Abduction posture
Phalange	Proximal	Middle	Distal	Proximal
ICP	0.55	0.88	0.89	0.36
Proposed method(single axis rotation)	0.63	0.96	1.06	0.44

Number of Subject = 2

Table 3. Thumb: average motion error at the time of each limit posture motion [mm].

Phalange	Metacarpal	Proximal	Distal
ICP	0.35	0.43	0.47
Proposed method(single axis rotation)	1.22	0.80	1.14
Proposed method (CMC: Quaternion interpolation, MP,IP: Single axis rotation)	0.35	0.47	0.96

Number of Subject = 2

Table 4. Average motion error at the time of product posture reproduction[mm].

	Brake grasp posture		
Phalange	Proximal(thumb: Metacarpal)	Middle(thumb: Proximal)	Distal
ICP	0.5	0.6	0.73
Proposed methodl	1.22	1.24	1.95

Number of Subject = 2

rotation became 0.80~1.22 mm, while those generated by our method (quartanion interpolation for CMC joint) were reduced to 0.35~0.96mm as shown in Fig.10. The difference in the error between the ICP and the single axis rotation became a maximum of 0.87mm, while the one between the ICP and our method were reduced to 0.49mm or less. Moreover, Table 4 shows the average motion error when reproducing a grasp posture for a product using the proposed bone link model. The average motion errors of all fingers in the proposed model were within 1.5mm. So, it can be said that the approximations grasp posture is reproducible with high precision.

As a result of these results, it can be said that the proposed joint modeling for the bone link model is precise enough for reproducing the virtual grasp postures.

Next, the skin surface deformation of the digital hand at the maximum flexion of thumb CMC joint is graphically shown in Fig. 11. Displacement distribution between the skin surface model of the digital hand and the real skin surface measured by MRI at this posture is shown in Table 5.

When only using the SSD(Fig. 11(a)) in the deformation, the skin swelling of the thumb's root is clearly insufficient. But the proposed skin deformation compensation by RBF enables our skin surface model to precisely reproduce the real swelling (Fig. 11(b)). As shown in Table 5, the average deformation errors were improved from 3.7mm to 0.6mm. Very precise deformation could be reproduced.

Finally, the contact area between the product model surface and the digital hand surface was verified in case of grasping a bicycle handle bar. Fig. 12(a) indicates a real contact area by a human subject obtained by stamping method in a real grasp experiment. Fig. 12(b) is a real grasp posture and estimated contact area (read and green) generated by a skin surface model extracted from the MRI measurement and the product mesh model. The contact area was extracted by collecting the vertices where distance between the skin

Table 5. Skin deformation distance error at the time of each thumb joint motion[mm].

Skin deformation method	Only SSD	After RBF interpolation
Flexion	7.0	0.6
Extension	4.5	0.6
Abduction	2.6	0.6
Adduction	2.9	0.6

Number of Subject = 2

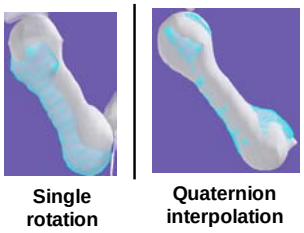

Fig. 10. The error of the metacarpal at the time of the thumb CMC joint motion reproduction.

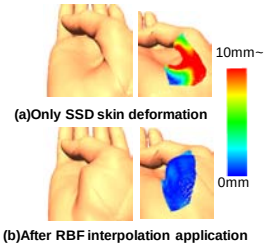

Fig. 11. Skin deformation at the time of the thumb CMC joint maximum flexion.

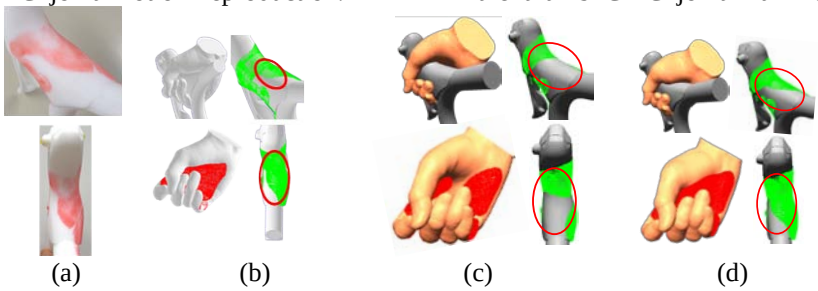

(a) (b) (c) (d)

Fig. 12. Contact area evaluation with the product. (a)Real product, (b)Estimated from MRI measure ment data, (c)Simulated by Digital hand (only SSD skin deformation),(d) Simulated by Digital hand (After RBF interpolation application).

surface model and the product model are less than 2.0mm. Fig. 12(c) indicates the simulated contact area between the digital hand and the product model using the same extraction criterion above when using the SSD only as the skin surface deformation. From Fig. 12(c), the swelling of the skin surface around the ball of the thumb was insufficient, and contact area on the product surface was evaluated too small. Meanwhile, from Fig. 12(d), when using the compensation by RBF, it was found that the swelling of the skin was well reproduced and the simulated contact area (green area in Fig. 12(d)) approximated the estimated contact area (Fig. 12(b)) and the real contact area (Fig. 12(a)) much better than those of Fig. 12(c).

Conclusions

A new method of MRI-based modeling of a digital hand was proposed whose precision was sufficient to reproduce virtual grasp postures for ergonomic assessments. The finger joint motion of the bone link model and the large skin surface deformation along with the finger flexion were modeled from MRI images. The proposed bone link model which enabled CMC joint motion with quaternion-based interpolation could reproduce the phalange motion within 1.06 mm error without grasp and within 1.95 mm error in case of grasp. The proposed skin surface model whose skin deformation was compensated by RBF interpolation could reproduce the real skin deformation within the 0.6mm error. The comparison of the simulated contact area of our hand model with the real one showed the effectiveness of the proposed model.

References

[1] N.S.Pollard, Closure and Quality Equivalence for Efficient Synthesis of Grasps from Examples, *International Journal of Robotics Research*, vol.23, no.6,595-613, 2004.

[2] Yui Endo , Satoshi Kanai, Natsuki Miyata, Makiko Kouchi and Masaaki Mochimaru, An Application of a Digital Hand to Ergonomic Assessment of Handheld Information Appliances, *SAE Technical Papers*, 2006-01-2325, 2006.

[3] Y. Li, et al., Data Driven Grasp Synthesis using Shape Matching and Task-Based Pruning, *IEEE Transactions on Visualization and Computer Graphics*, vol.13, no.4, 732-747, 2007

[4] J. Yang et al., Posture Prediction and Force/Torque Analysis for Human Hands, *Proceedings of the SAE 2006 Digital Human Modeling for Design and Engineering Conference*, 2006-01-2326, 2006.

[5] N.Miyata et al., Posture Estimation for Design Alternative Screening by DhaibaHand – Cell Phone Operation, *Proceedings of the SAE 2006 Digital Human Modeling for Design and Engineering Conference*, 2006-01-2327, 2006.

[6] Yui Endo, Satoshi Kanai, Takeshi Kishinami, Natsuki Miyata, Makiko Kouchi, Masaaki Mochimaru, Virtual Ergonomic Assessment on Handheld Products based on Virtual Grasping by Digital Hand, *SAE 2007 Transactions Journal of Passenger Cars: Electronic and Electrical Systems*, Vol.116. No.7, pp.877-887, 2008.

[7] Yui Endo, Satoshi Kanai, Takeshi Kishinami, Natsuki Miyata, Makiko Kouchi, Masaaki Mochimaru, Optimization-Based Grasp Posture Generation Method of Digital Hand for Virtual Ergonomic Assessment, *SAE International Journal of Passenger Cars -Electronic and Electrical Systems*, Vol.1 No.1, pp.590-598, 2009.

[8] M.Kouchi et al., An Analysis of Hand Measurements for obtaining representative Japanese Hand Models, *Proceedings of the 8th Annual Digital Human Modeling for Design and Engineering Symposium*, 2005-01-2734, 2005.

[9] T. Kurihara, and N. Miyata, Modeling Deformable Human Hands from Medical Images, *Eurographics/ACM SIGGRAPH Symposium on Computer Animation*, pp.355-363, 2004.

[10] N. Miyata, M. Kouchi, M. Mochimaru, and T. Kurihara, Finger Joint Kinematics from MR Images, *IEEE International Conference on Intelligent Robots and Systems*, pp.4110-4115, 2005.

[11] A.I.Kapandji, *The Physiology Of The Joints, Volume 1: The Upper Limb*, Churchill Livingstone, 2005.

[12] Osirix, http://www.osirix-viewer.com/

[13] Geomagic, http://www.geomagic.com/en/